

# 2-D Modeling and Calculations of Stratospheric Ozone and Influences of Convection, Diffusion, and Time

Ibraheem Alelmi<sup>1</sup>, Laurie Wei<sup>1</sup>, Sen Nieh<sup>2,3\*</sup>

<sup>1</sup>Department of Mechanical Engineering, The Catholic University of America, Washington, DC, USA

<sup>2</sup>School of Engineering, The Catholic University of America, Washington, DC, USA

<sup>3</sup>College of Engineering, Yuan Ze University, Taoyuan

Email: \*nieh@cua.edu

**How to cite this paper:** Alelmi, I., Wei, L. and Nieh, S. (2024) 2-D Modeling and Calculations of Stratospheric Ozone and Influences of Convection, Diffusion, and Time. *Atmospheric and Climate Sciences*, 14, 250-276.

<https://doi.org/10.4236/acs.2024.142016>

**Received:** March 8, 2024

**Accepted:** April 19, 2024

**Published:** April 22, 2024

Copyright © 2024 by author(s) and Scientific Research Publishing Inc. This work is licensed under the Creative Commons Attribution International License (CC BY 4.0).

<http://creativecommons.org/licenses/by/4.0/>



Open Access

---

## Abstract

An engineering system approach of 2-D cylindrical model of transient mass balance calculations of ozone and other concerned chemicals along with fourteen photolysis, ozone-generating and ozone-depleting chemical reaction equations was developed, validated, and used for studying the ozone concentrations, distribution and peak of the layer, ozone depletion and total ozone abundance in the stratosphere. The calculated ozone concentrations and profile at both the Equator and a 60°N location were found to follow closely with the measured data. The calculated average ozone concentration was within 1% of the measured average, and the deviation of ozone profiles was within 14%. The monthly evolution of stratospheric ozone concentrations and distribution above the Equator was studied with results discussed in details. The influences of slow air movement in both altitudinal and radial directions on ozone concentrations and profile in the stratosphere were explored and discussed. Parametric studies of the influences of gas diffusivities of ozone  $D_{O_3}$  and active atomic oxygen  $D_O$  on ozone concentrations and distributions were also studied and delineated. Having both influences through physical diffusion and chemical reactions, the diffusivity (and diffusion) of atomic oxygen  $D_O$  was found to be more sensitive and important than that of ozone  $D_{O_3}$  on ozone concentrations and distribution. The 2-D ozone model present in this paper for stratospheric ozone and its layer and depletion is shown to be robust, convenient, efficient, and executable for analyzing the complex ozone phenomena in the stratosphere.

## Keywords

Stratospheric Ozone, 2-D Model, Ozone Layer, Ozone Depletion, Convection, Diffusion

## 1. Introduction

The atmosphere of the Earth is stratified into troposphere, stratosphere, mesosphere, and thermosphere. The stratosphere extends from approximately 10 km above the Earth surface to about 50 km, where the protective layers of ozone and greenhouse gases reside in air. This thin ozone (O<sub>3</sub>) layer plays a crucial role as a guardian, absorbing harmful ultraviolet (UV) rays and ensuring the safety of all living beings on the ground. The Sun emits three types of UV radiation: higher-energy UV-C with wavelengths of 100 to 280 nm, UV-B with wavelengths of 280 to 315 nm, and lower-energy UV-A with wavelengths of 315 to 400 nm, which collectively amount to about 9% of total solar energy [1] [2]. UV-C radiation is extremely hazardous to all forms of life and fortunately is entirely absorbed by the stratospheric ozone layer. Being known to cause skin cancer, cataracts, and a weakened immune system of humans, UV-B radiation is substantially absorbed by this ozone layer. UV-A radiation, on the other hand, is mostly unaffected by the ozone layer. The UV-A can be beneficial for the production of a vital nutrient (vitamin D) and bone health. However, overexposure to UV-A may cause sunburn, premature aging of skin, and even skin cancer. Acting as a natural sunscreen, the ozone layer absorbs approximately 90% of the UV rays and safeguards all living organisms. Generally, about 90% of the total ozone resides in the stratosphere as a “good” protective ozone, while the remaining 10% of the total ozone residing in the troposphere, particularly near the Earth’s surface, is a polluting “bad” ozone, contributing to the photochemical smog [1] [3] [4].

In the mid-1980s, scientists identified an alarming thinning of the ozone layer over Antarctica, leading to widespread concerns among the scientific community and governments worldwide. Nearly 100 ozone-depleting substances were pinpointed as culprits in the depletion of stratospheric ozone. These chemicals fall into three categories: chlorine (Cl) gases, bromine (Br) gases, and nitrogen oxides (NO<sub>x</sub>), each with varying atmospheric concentrations and impacts [5] [6]. Many of the chlorine-containing chemicals originated from traditional refrigerants like chlorofluorocarbons (CFCs) and hydrochlorofluorocarbons (HCFCs), which were widely used in the late 20th century in approximately 1.4 billion air conditioners and 0.7 billion refrigerators in the world. The bromine-containing chemicals, such as methyl bromide (CH<sub>3</sub>Br) and halons, used commonly for fires extinguishing and for large computer, hardware, and engine protections [6] [7]. Both thermal-NO<sub>x</sub> and fuel-NO<sub>x</sub>, such as NO and NO<sub>2</sub>, are a family of poisonous, highly reactive gases, coming primarily from combustion of fossil fuels, for generating about 80% of the global electricity, and for use in air, sea, and land transportation, including about 1.3 billion cars/trucks and 0.7 billion motorcycles used every day and everywhere in the world today.

Guided by Prof. Crutzen in the 1980s, scientists Molina and Rowland made a ground breaking discovery through laboratory experiments and computational modeling, for establishing a critical link between chlorofluoromethane and the

ozone hole. This landmark finding earned them the Nobel Prize in Chemistry in 1995 [8] [9]. The global distribution of stratospheric ozone is influenced by numerous factors, such as geographical location, altitude, time of the day and month of the year, atmospheric air motion, and the presence and amount of different ozone-depleting chemicals. The total ozone abundance above a specific location typically ranges from 200 to 500 Dobson Units (DU), with a global average of 300 DU [1] [5] [9]. The solar radiation, including UV rays, is most intense and long in the tropical areas, where it generates atomic oxygen O by photolysis. Atomic oxygen collides with abundance oxygen molecules O<sub>2</sub> and produces ozone molecules O<sub>3</sub> [1] [10]. However, ozone concentrations are found to be lower above the equator and higher in the mid-latitudes and polar region. This observation is attributed to the gradual large-scale horizontal circulation of ozone-rich tropical stratospheric air towards the polar regions [1] [8], contributing to variations in ozone levels across different latitudinal zones on Earth.

In the study of atmospheric dynamics, several modeling and numerical tools were developed and employed to investigate various atmospheric phenomena, including the ozone layer. While two-dimensional (2-D) models have received primary attention, the importance of simpler 1-D models should not be underestimated, as they often provide specific insights into ozone concentrations, the stratospheric ozone layer, and ozone depletion mechanisms [2] [6] [11]. Among the 2-D models, the 2-D chemical models have aimed to incorporate the effects of circulation and mixing. Utilizing grids to represent latitude and altitude, these models offer insights into average conditions across latitude bands, primarily in the high stratosphere, but they face limitations in representing turbulence in less uniform regions like the lower stratosphere. Nevertheless, despite these challenges, 2-D models remain valuable tools for understanding radiative-chemical interactions and enhancing our knowledge of spatial distribution dynamics, all while maintaining simplicity [11] [12] [13].

Another 2-D approach is the use of zonal mean models, which divide the atmosphere into latitude bands to compute average ozone concentrations. These models, characterized by their simplicity, are computationally efficient and easy to set up, enabling the study of large-scale trends and patterns. However, they have limitations, such as not accounting for regional variations in ozone concentration or the influence of atmospheric circulation patterns [14]. To gain a more comprehensive understanding of ozone layer dynamics and behavior, it is essential to combine zonal mean models with other models and observational data. Numerical Weather Prediction models, designed for weather forecasting, have yet to fully incorporate ongoing chemical changes in the atmosphere [15]. These models consider air and water properties from a physical perspective, including the transfer of momentum, heat, mass, and humidity in the atmosphere through parameterizations due to computational constraints. Despite their complexity, Numerical Weather Prediction models do not account for chemical alterations in the atmosphere, highlighting the need for further enhancements to improve their accuracy in long-term forecasts [16].

This paper seeks to provide a more comprehensive study of stratospheric ozone dynamics and the crucial processes of ozone layer and holes in global atmospheric changes. By employing an engineering system approach, we have developed a 2-D ozone model in a cylindrical coordinate system [7]. Our primary objective is to model and calculate ozone concentrations, layer profile, and depletion processes, considering the different competing physical-chemical-radiative processes: wind convection, mass diffusion, UV photolysis, ozone-producing and ozone-depleting chemical reactions. Notably, our study stands out by integrating conservation equations of substances of ozone and concerned chemical species under transient, convective, diffusive, and reactive processes in a cylindrical coordinate framework. It offers advantages in terms of computational speed and memory capacity, and focused analyses on specific geographical region, such as South and North poles. This paper is to present our ongoing modeling, validation, and simulation efforts, and the preliminary findings to help better understand the stratospheric ozone behavior and depletion processes.

## 2. Modeling and Numerical Methods

### 2.1. Conservation of Mass Equations

In the study of stratospheric ozone concentration, distribution of layer, and ozone depletion and ozone hole, we utilize a system approach involving 2-D cylindrical mass balance equations [7] [17]. The conservation equations of various substances  $C_i$  [concentration, in mass or molecules per unit volume, or parts per million, ppm], such as ozone  $O_3$ , atomic oxygen  $O$ , and various concerned chemical species, include the change with time ( $\frac{\partial C_i}{\partial t}$ ), convective transport due to slow air movement ( $U \cdot \nabla C_i$ ), [ $U$  being the velocity of air motion], mass diffusion due to concentration gradients ( $D_i \nabla^2 C_i$ ) [ $D_i$  being the diffusivity of species  $C_i$ ], and various chemical reactions ( $\frac{d[C_i]}{dt}$ ), from photolysis, ozone-generation, and ozone-depletion reactions. The conservation of mass equations below are coupled partial differential equations in a transient axisymmetric cylindrical coordinate ( $t, r, z$ ), governing the evolving changes of a species in the stratosphere, encompassing five simultaneous and competing processes: convective transport, mass diffusion, photo-dissociation, ozone-generating reactions, and ozone-depleting reactions.

Conservation of Mass Equations:

$$\frac{\partial C_i}{\partial t} = \frac{1}{r} \frac{\partial}{\partial r} \left[ \left( D_i \frac{\partial C_i}{\partial r} \right) r \right] - U_r C_i r + \frac{\partial}{\partial z} \left( D_i \frac{\partial C_i}{\partial z} - U_z C_i \right) + \frac{d[C_i]}{dt}$$

For the simplicity, the equations above encapsulate the key processes and parameters, but assume axisymmetry (*i.e.*,  $\partial C_i / \partial \phi = 0$ ). The concentration of a species  $C_i$  generally changes with time  $t$ , altitude  $z$ , and radial position  $r$ . The altitude or elevation of interests is the stratosphere, extending from  $z = 10$  km to  $z = 50$  km, radial coordinate ( $r$ ) being of different ranges and values, time ( $t$ ) of in-

terests being in seconds, days, or months, the slow wind speeds in the  $z$  and  $r$  directions being  $U_z$  and  $U_r$ , and diffusivity of  $C_i$  gases being  $D_i$ . The concentration  $C_i$  (in ppm or in molecules/volume) of species gases can be regular oxygen  $O_2$ , naturally available ozone  $O_3$ , atomic oxygen  $O$  from photolysis, and various man-induced ozone depleting chemicals, such as  $Cl$ ,  $ClO$ ,  $ClOClO$ ,  $ClOO$ ,  $Br$ ,  $BrO$ ,  $BrCl$ ,  $NO$ , and  $NO_2$ .

In order to provide insight into various chemical reactions contributing to the change of ozone  $O_3$ , or in general,  $\frac{d[C_i]}{dt}$ , **Table 1** lists a comprehensive compilation of 14 possible chemical reactions, its respective reaction rate constants  $k_i$ , initial concentrations  $C_i$ , and reaction expressions  $r_i$ , that are directly relevant to our study.

Equations (1), (2) and (3) illustrate the Chapman mechanism, first introduced in 1930 [10]. This mechanism elucidates the natural processes governing ozone generation and consumption in the absence of human-induced ozone-depleting substances. These processes involve photo-excitation, collision-induced transformation, and dissociation. The non-reactive species, denoted as “M”, serves as a random stabilizing intermediate, such as molecules  $N_2$  [19]. In the stratosphere,

**Table 1.** List of total 14 natural and man-induced chemical equations, reaction rate constants  $k_i$ , initial concentrations of different species  $C_i$ , and reaction expression  $r_i$  of Equations (1) to (14) [7] [18] [19].

Eq. No.	Reaction Equations	Reaction Rate Constants ( $k_i$ ) ( $cm^3/molecules*s$ )	Initial Concentrations of $C_i$ ( $molecules/cm^3$ )	Reaction Expression ( $r_i$ )
1	$O_2 + hv(\text{sunlight}) \rightarrow 2O^*$	$k_1 = 1.03 \times 10^{-94}$	$O_2 = 2.00 \times 10^{17}$	$r_1 = k_1 [O_2]$
2	$O^* + O_2 + M \rightarrow O_3 + M$	$k_2 = 5.92 \times 10^{-34}$	$O = 1.00 \times 10^{-6}$	$r_2 = k_2 [O_2] [O]$
3	$O_3 + hv(\text{sunlight}) \rightarrow O_2 + O^*$	$k_3 = 4.38 \times 10^{-26}$	$O_3 = 5.00 \times 10^{12}$	$r_3 = k_3 [O_3]$
4	$Cl + O_3 \rightarrow ClO + O_2$	$k_4 = 1.22 \times 10^{-11}$	$Cl = 6.46 \times 10^4$	$r_4 = k_4 [O_3] [Cl]$
5	$ClO + O \rightarrow Cl + O_2$	$k_5 = 3.80 \times 10^{-11}$	$ClO = 7.22 \times 10^7$	$r_5 = k_5 [O] [ClO]$
6	$ClO + ClO + M \rightarrow (ClO)_2 + M$	$k_6 = 2.16 \times 10^{-32}$		$r_6 = k_6 [ClO]^2$
7	$(ClO)_2 + hv(\text{sunlight}) \rightarrow Cl + ClOO$	$k_7 = 8.53 \times 10^{-15}$	$(ClO)_2 = 1.00 \times 10^{-6}$	$r_7 = k_7 [(ClO)_2]$
8	$ClOO + M \rightarrow Cl + O_2 + M$	$k_8 = 6.51 \times 10^{-13}$	$ClOO = 1.00 \times 10^{-6}$	$r_8 = k_8 [ClOO]$
9	$NO + O_3 \rightarrow NO_2 + O_2$	$k_9 = 1.78 \times 10^{-14}$	$NO = 1.00 \times 10^9$	$r_9 = k_9 [O_3] [NO]$
10	$NO_2 + O \rightarrow NO + O_2$	$k_{10} = 1.05 \times 10^{-11}$		$r_{10} = k_{10} [NO_2] [O]$
11	$NO_2 + O_3 \rightarrow NO + 2O_2$	$k_{11} = 1.00 \times 10^{-18}$	$NO_2 = 1.00 \times 10^9$	$r_{11} = k_{11} [NO_2] [O_3]$
12	$Br + O_3 \rightarrow BrO + O_2$	$k_{12} = 1.18 \times 10^{-12}$	$Br = 3.2 \times 10^5$	$r_{12} = k_{12} [Br] [O_3]$
13	$BrO + ClO \rightarrow BrCl + O_2$	$k_{13} = 1.02 \times 10^{-12}$	$BrO = 6.4 \times 10^6$	$r_{13} = k_{13} [BrO] [ClO]$
14	$BrCl + hv(\text{sunlight}) \rightarrow Br + Cl$	$k_{14} = 1.06 \times 10^{-8}$	$BrCl = 1.00 \times 10^{-6}$	$r_{14} = k_{14} [Br] [Cl]$

ozone  $O_3$  forms through multiple steps of chemical process initiated by sunlight's UV radiation. This high energy ray causes the dissociation of the abundant oxygen molecules  $O_2$  into active oxygen atoms  $O + O$ , which subsequently collides with regular oxygen molecules to form ozone  $O_3$ . Since the concentration of molecular oxygen  $O_2$  is very large, constituting 20.95% or  $2.095 \times 10^5$  ppm in air, the generation of ozone  $O_3$  primarily depends on the availability of atomic oxygen  $O$ .

Equations (4) to (14) outline three potential ozone-depleting reaction cycles resulted from human-induced ozone-depleting substances [19] [20]. Equations (4) to (8) describe how chlorine-containing compounds, such as traditional refrigerants CFCs and HCFCs, participate in converting ozone  $O_3$  into regular oxygen molecules  $O_2$ . Chlorine-containing gases act as a catalyst for ozone depletion reactions, including  $Cl$ ,  $ClO$ ,  $ClOO$ , and  $(ClO)^2$ , which are re-formed each time the depleting cycle is completed, and hence available for further destruction of ozone. Equations (4) and (5) are more important at tropical and middle latitude regions, where UV radiation is more intense. Equations (6), (7), (8), and (4), are more important for Antarctica, where  $ClO$  can reach large values during late winter and early spring, and the abundant  $ClO$  can react with another  $ClO$  to initiate the destruction of ozone [1].

Equations (9), (10), and (11) elucidate how nitrogen oxides  $NO_x$  (both  $NO$  and  $NO_2$ ), resulted from burning of fossil fuels [21] [22] or from natural processes, such as wild forest fires, can react with ozone  $O_3$  and reduce it to regular oxygen  $O_2$ , when  $NO_x$  accumulated and transported from the troposphere to the stratosphere via upward air motion. Also important for the polar region are Equations (12), (13), and (14), that expound on how bromine-containing chemicals, such as methyl bromide ( $CH_3Br$ ) and halons, initially developed for fire suppression and subsequently used in large-scale applications like computer hardware and engine protection [1] [19], can similarly contribute to the destruction of ozone  $O_3$  into regular oxygen  $O_2$ . Like chlorine, bromine also functions as an ozone-depleting catalyst, as active bromine-containing gases, including  $Br$ ,  $BrO$ , and  $BrCl$ , which are re-formed each time the depleting cycle is completed, and hence available for further destruction of ozone. Since the sunlight (UV) is required for both Equations (7) and (14), during polar night and other periods of darkness, ozone won't be destroyed by these reactions [1].

**Table 1** provides pertinent published data, including reaction rate constants ( $k_i$ ) and initial concentrations for chemical species in Equations (1) to (14) for the tropical regions [19]. It should be noted that these values may vary with factors such as latitude, time, and environment conditions. From the reaction expressions ( $r_i$ ) in **Table 1**, we can derive for the total reaction rate for a species  $\frac{d[C_i]}{dt}$ , including ozone concentration  $\frac{d[O_3]}{dt}$  and consequently the ozone layer characteristics, atomic oxygen  $O$ , and various ozone depleting chemicals:  $Cl$ ,  $ClO$ ,  $Br$ ,  $BrO$ ,  $NO$ ,  $NO_2$ , etc. For instance,  $\frac{d[O_3]}{dt} = r_2 - r_3 - r_4 - r_9 - r_{11} - r_{12}$

and  $\frac{d[\text{O}]}{dt} = 2r_1 - r_2 + r_3 - r_5 - r_{10}$ . As we add the reaction terms  $\frac{d[C_i]}{dt}$  into the mass balance equations, along with the transient term  $(\frac{\partial C_i}{\partial t})$ , diffusion and convection terms in cylindrical coordinate, we get the governing equations for solving for concentrations and changes of ozone and other concerned species in the stratosphere. Our 2-D ozone model enables the study the ozone dynamics, ozone layer and ozone hole under various natural and man-induced depletion reactions at different geographical locations, times of the day or months of the year, and environment and boundary conditions [7] [20].

## 2.2. Numerical Methods

In the mass balance equations, the concentrations of ozone and other species are a function of time ( $t$ ), radial position ( $r$ ), and altitude/elevation ( $z$ ), denoted as  $[C_i]$  or  $[\text{O}_3] = f(t, r, z)$ . For the mass balance equations, we'll assume axisymmetric ( $\partial C_i / \partial \phi = 0$ ) for the sake of simplicity, select property and environment constants,  $k_i^s, D_b, U_z, U_r$  from the published measured or known data, and consider at different boundary and initial conditions in the stratosphere. The axisymmetric assumption allows us to solve the equations within a single plane of  $r - z$ , rotating cylindrically, which neglects the variations in polar or azimuthal angles. This approach provides acceptable results for a region of smaller radius on the globe and produces good results for the stratosphere above the polar region of varying size/radius.

To approximate the simultaneous partial differential equations into a very large, but manageable system of simultaneous algebraic equations, we employ finite difference formulas to represent the first- and second-order partial derivatives in both spatial coordinates,  $r$  and  $z$ , and temporal coordinate,  $t$ . The discretization of the solution domain results in a grid-based representation with chosen values of  $\Delta t$ ,  $\Delta r$ , and  $\Delta z$  in the stratosphere [23] [24] [25]. The first-order

partial derivatives are expressed as  $\frac{\partial C_i}{\partial t} = \frac{C_{i(i,j,n+1)} - C_{i(i,j,n-1)}}{2\Delta t}$ ,

$\frac{\partial C_i}{\partial r} = \frac{C_{i(i,j+1,n)} - C_{i(i,j-1,n)}}{2\Delta r}$ , and  $\frac{\partial C_i}{\partial z} = \frac{C_{i(i+1,j,n)} - C_{i(i-1,j,n)}}{2\Delta z}$ , while the second-order

partial derivatives expressed as,  $\frac{\partial^2 C_i}{\partial r^2} = \frac{C_{i(i+1,j,n)} - 2C_{i(i,j,n)} + C_{i(i-1,j,n)}}{\Delta r^2}$  and

$\frac{\partial^2 C_i}{\partial z^2} = \frac{C_{i(i,j+1,n)} - 2C_{i(i,j,n)} + C_{i(i,j-1,n)}}{\Delta z^2}$ . The numerical solution process involves

formulating time-dependent convection-diffusion finite difference equations, which are applied separately to ozone  $\text{O}_3$ , molecular oxygen  $\text{O}_2$ , atomic oxygen  $\text{O}$ , and other relevant chemical species. Notably, we can safely omit the mass balance equation for molecular oxygen  $\text{O}_2$  due to its large and stable concentration of 20.95% in the atmosphere, which remains largely unaffected by changes in small gas concentrations, typically measured in several ppm. To account for chemical reactions, we add the last term,  $\frac{d[C_i]}{dt}$ , representing the overall chem-

ical reaction of linear algebraic equations, as listed in details in **Table 1**.

We systematically set up a large set of simultaneous finite difference algebraic equations for all grid meshes within the stratosphere, as given in Equation (15) below, where the term on the left and the 1<sup>st</sup> term on the right representing the transient change of ozone concentration, the 2<sup>nd</sup>, 3<sup>rd</sup>, and 6<sup>th</sup> terms on the right representing the mass diffusion due to concentration gradients, the 4<sup>th</sup>, 5<sup>th</sup>, and 7<sup>th</sup> on the right representing the transport by advection from slow air movement, and the last (8<sup>th</sup>) term on the right representing the overall change of ozone by various ozone-depleting and ozone-producing chemical reactions.

$$\begin{aligned}
 O_3^{n+1}{}_{i,j} = O_3^n{}_{i,j} + \Delta t * \left\{ \frac{1}{r} \left[ \frac{D_i}{\Delta r^2} r (O_3^n{}_{i+1,j} - 2O_3^n{}_{i,j} + O_3^n{}_{i-1,j}) \right. \right. \\
 + \frac{D_i}{2\Delta r} (O_3^n{}_{i+1,j} - O_3^n{}_{i-1,j}) - \frac{U_r}{2\Delta r} r (O_3^n{}_{i+1,j} - O_3^n{}_{i-1,j}) - U_r O_3^n{}_{i,j} \left. \right] \\
 + \left[ \frac{D_i}{\Delta z^2} (O_3^n{}_{i,j+1} - 2O_3^n{}_{i,j} + O_3^n{}_{i,j-1}) - \frac{U_z}{2\Delta r} (O_3^n{}_{i,j+1} - O_3^n{}_{i,j-1}) \right] \left. \right\} \\
 + \Delta t * \frac{d[O_3^n]}{dt}
 \end{aligned} \quad (15)$$

where,

- $\Delta t$ : time step interval for numerical calculations.
- $\Delta r$  and  $\Delta z$ : spatial grid intervals in the radial and vertical directions, respectively.
- $D_i$ : diffusivity of species  $i$
- $U_r$  and  $U_z$ : radial and vertical air movement velocities, respectively.
- $\frac{d[O_3^n]}{dt}$ : rate of change of ozone concentration over time, resulted from the various chemical reactions. For example, for ozone,

$$\frac{d[O_3]}{dt} = r_2 - r_3 - r_4 - r_9 - r_{11} - r_{12} \quad \text{and for atomic oxygen,}$$

$$\frac{d[O]}{dt} = 2r_1 - r_2 + r_3 - r_5 - r_{10} \quad (r_i\text{'s being listed in Table 1}).$$

These equations account for the overall changes in ozone concentration due to various natural and man-induced chemical reactions in the stratosphere, including both generation and depletion mechanisms. For our numerical solutions, we utilized Python Solvers, which provide a robust environment for solving complex systems of simultaneous equations. Python, with its extensive libraries for numerical computations, served as the ideal software for executing our code. In our simulations, we discretized the altitude (elevation)  $z$  into intervals of  $\Delta z$  ranging from 1 km to 2 km, or as dimensionless altitude either using  $z^* = (z - 15)/(45 - 15)$  or using  $z^* = (z - 10)/(50 - 10)$ , depending on the available measured or known data for comparison. The dimensionless radial coordinate,  $r^*$ , was selected within a range of 50 km or larger, with discretization of  $\Delta r$  between 1 km, 2 km, or larger. The time step  $\Delta t$  has been tested with different values, ranging from 0.1 second to 10 seconds, to ensure computational conver-

gence, efficiency, and stability. A value of  $\Delta t = 1$  second was ultimately chosen to capture the dynamic changes in ozone concentration with a good temporal resolution. Consequently, most of the results presented in this paper were obtained using  $\Delta t = 1$  second,  $\Delta z = 2$  km (or 20 grids along  $z^*$  direction), and 20 grids along the radial direction ( $r^* = 0$  to 1.0).

### 3. Results and Discussions

#### 3.1. Validation of 2-D Ozone Model

In our earlier published paper [7], we examined the validation of our 2-D Ozone Model from both chemical and physical aspects with the available measured, analytical, or calculated results of ozone dynamics in the stratosphere. Considering catalytic depletion reactions by chlorine from CFCs and  $\text{NO}_x$ , but with negligible diffusion and convection, our calculated transient ozone concentrations under the same boundary conditions and rate constants closely matched with results of Fogler's Ozone Depletion Model [7] [19]. The agreement of within 4% difference showed our 2-D model is reliable in capturing the complex ozone depletion reactions. Also, considering convective and diffusive dispersion, but with negligible chemical-photolysis reactions, our calculated transient ozone distributions closely matched with the published analytical solutions [7] [26]. The agreement is within only 0.1% difference.

In this paper, we further validate our 2-D Ozone Model with concurrent and competing processes of convection, diffusion, photolysis, and ozone-generating and ozone-depleting chemical reactions. The capabilities in data presentation and flexibilities in simulation of complex stratospheric ozone dynamics can also be seen. **Figure 1** shows the temporal and spatial evolution of dimensionless ozone concentrations from deep blue at 0.0 to max ozone of deep red at 1.0 (equivalent to  $[\text{O}_3] = 10$  ppm) on a  $r$ - $z$  plane from the month of June to month of August at the Equator caused primarily by convection and diffusion.

In **Figure 1**, the top left diagram, **Figure 1(a)**, represents the measured ozone contour in 2-D color plot at the Equator and is also the initial ozone concentrations for the simulation [27]. The top right diagram, **Figure 1(b)**, illustrates the same measured ozone distributions visualized in  $(r, z, \text{O}_3)$  3-D contour plot, where the peak ozone appears near the center of mid-altitude and mid-radial location in the stratosphere. The bottom left diagram, **Figure 1(c)**, displays the calculated ozone concentrations in 2-D contour plot after two months of time evolution to August, or after 90% of the total elapsed simulation time. The bottom right diagram, **Figure 1(d)**, presents the calculated ozone distributions in August at the Equator, where the peak value of ozone reduced to about 1/3 of that of June and the peak location shifted to higher altitude and radial place due to wind convection and mass diffusion.

In this calculation, both average dimensionless convective speeds,  $U_z$  and  $U_r$ , were taken at  $1 \times 10^{-8}$ , or a slow wind speed of 10 m/hr, with a reference length of 30 km and a reference time of 0.1 second. The total computation efforts

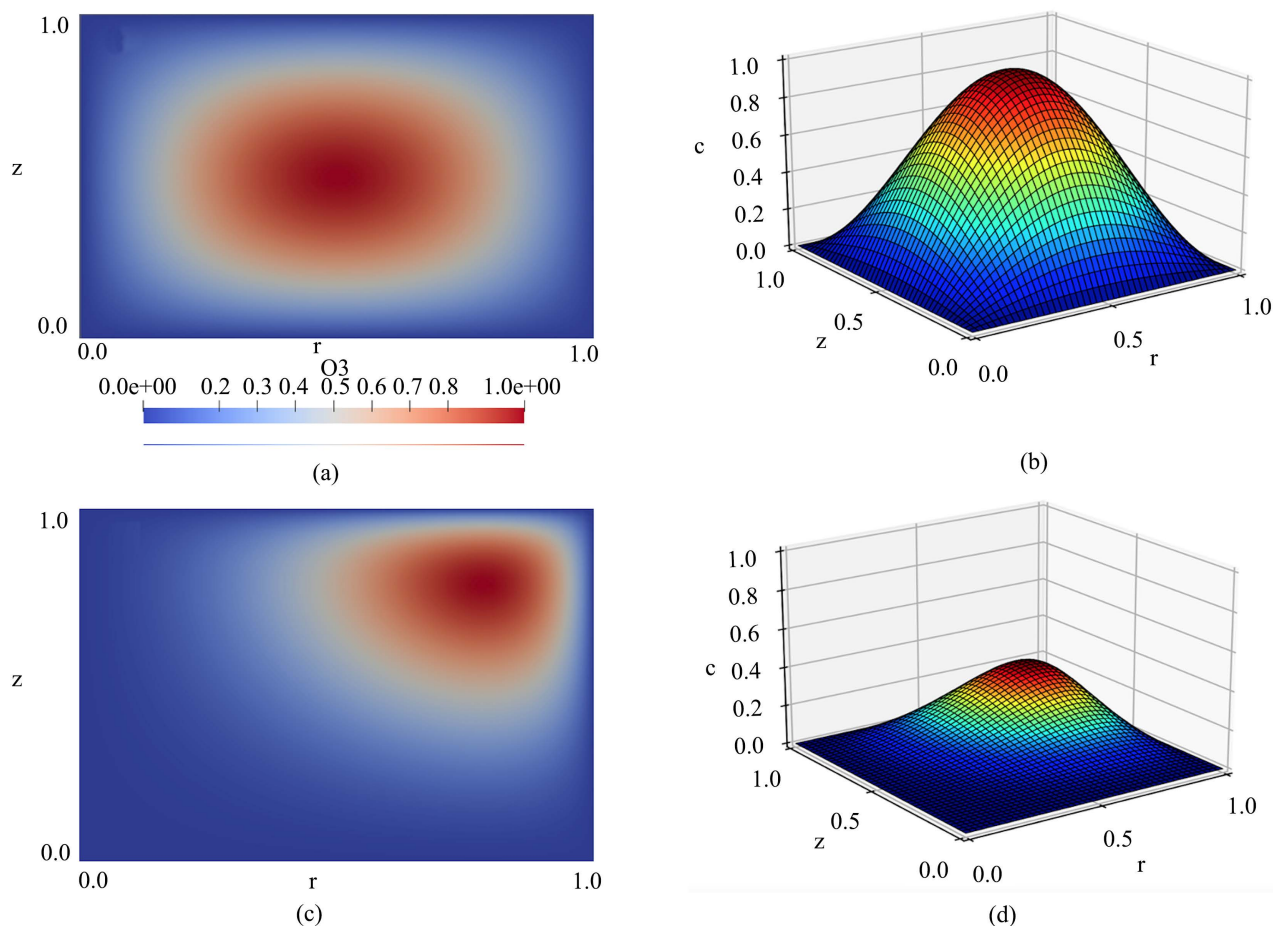


**Figure 1.** Temporal and spatial evolution of dimensionless ozone concentrations and distribution contour on r-z plane at the Equator from month of June to month of August, caused primarily by convection and diffusion.

spanned for more than two months with a time step of  $\Delta t = 1$  sec, or a total of  $5.2 \times 10^6$  steps/2-month, which took about 2 days of computational time by our laptop computer. It is evidently noted in the bottom figures that the peak ozone location shifted from the center of r-z plane to the right upper corner of the plane. The shift of ozone layer in the stratosphere is resulted from the dynamic interplay of convection and diffusion processes, along with weak chemical reactions.

**Figure 2** shows the global stratospheric ozone concentrations extracted from the measured data using the Microwave Limb Sounder [27], from the North Pole at  $90^\circ\text{N}$ , to the Equator, and to the South Pole at  $90^\circ\text{S}$ , for the month of June averaged over 15 years, from 2005 to 2019. The left diagram is the measured ozone concentrations in 2-D color plot and the right diagram being the same measured ozone distributions visualized in 3-D contour plot. **Figure 2** provides valuable insights into the long-term, larger-scale distribution and variations of ozone concentration on a global scale. Complementing the localized ozone observations in **Figure 1**, they can contribute to our comprehensive understanding of ozone behavior, both locally and globally.

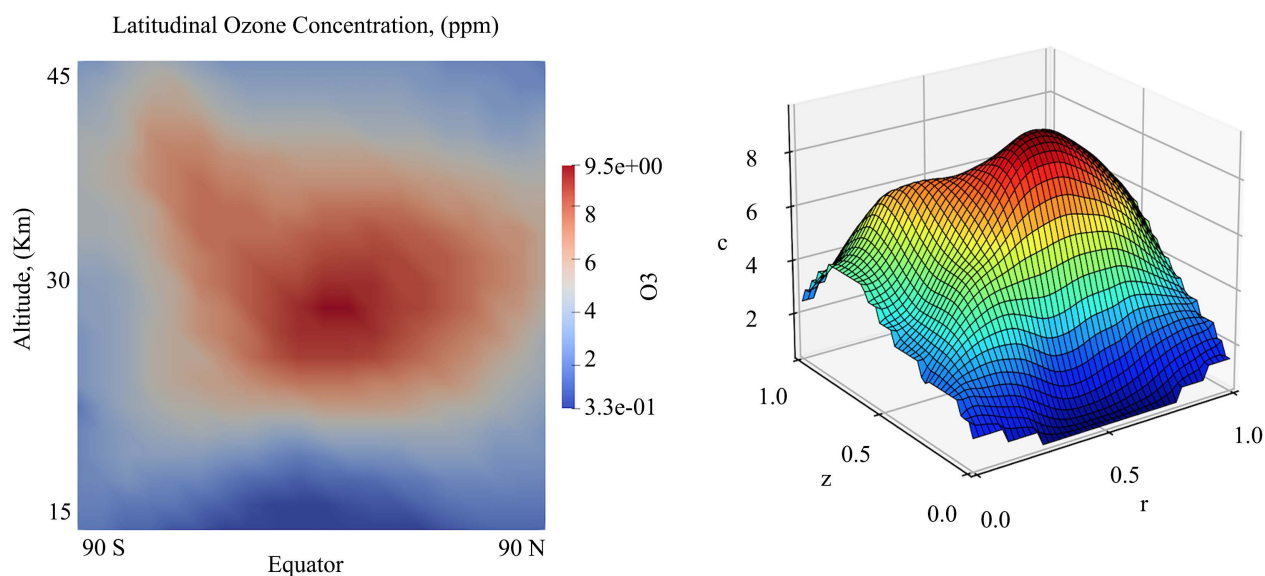


**Figure 2.** The measured global ozone concentrations along the altitude of the stratosphere from the North Pole 90°N, to the Equator, and to the South Pole 90°S, for the month of June averaged over 15 years, from 2005 to 2019 [27]. The left diagram is the measured ozone concentrations in 2-D color plot and the right diagram being the same measured ozone distributions visualized in 3-D contour plot.

**Figure 3** shows the comparison of the calculated ozone concentrations and distribution (solid curves) with the measured data (dotted curves) at two particular geographical locations: the Equator (near Singapore, blue curves) and the 60°N (at Oslo, Norway or Gulf of Alaska, USA, red curves). The equatorial region, known for its intense and long radiation from the Sun, provides an ideal place for studying ozone dynamics and the impact of UV radiation levels. On the other hand, the choice of 60°N allows us to explore distinct ozone dynamics and layer under different solar radiation and environmental conditions.

At the Equator, the solar radiation (UV ray and photolysis) is intense and prolonged. The calculated ozone concentrations (solid blue curve) exhibited a more symmetrical distribution along the altitude with a peak concentration of 9.41 ppm near the mid-altitude around  $z = 30$  km, shown in **Figure 3**. The measured ozone concentrations (dotted blue curve) exhibited a similar symmetrical distribution with a peak concentration of 9.76 ppm near  $z = 30$  km [27]. The calculated results of our 2-D ozone model generally followed the measured concentrations with the calculated average ozone concentration of 5.77 ppm, being very close to the measured average of 5.66 ppm. The ozone distribution profiles follow the same trend but with a coefficient of variation, or the average deviation, of 13.7%.

At the top boundary of the stratosphere at  $z = 45$  km above the Equator, the ozone concentration was taken as 3 ppm, based on the published measured value [27]. As the sunlight, particularly high-energy UV-C and UV-B, beams through the upper stratosphere, it breaks down the abundance oxygen molecules  $O_2$  into atomic oxygen O. These active oxygen atoms collide with abundance  $O_2$  to form ozone  $O_3$ , as shown in Equations (1) and (2) in **Table 1**. The processes continue

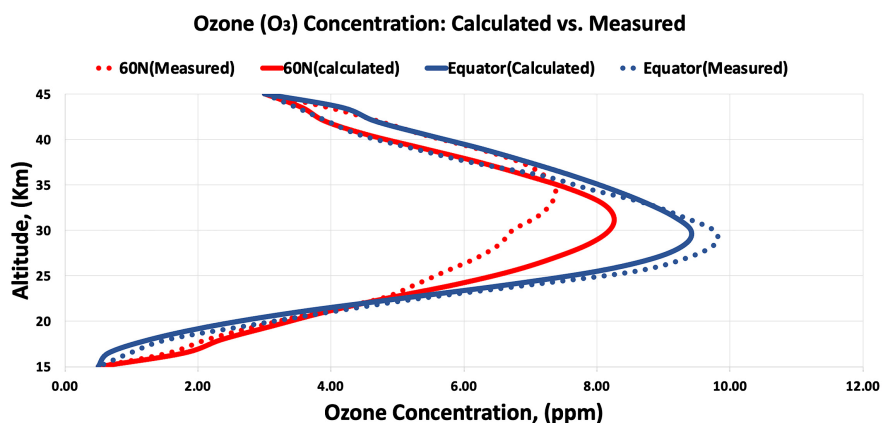


**Figure 3.** Comparison of calculated ozone concentrations and distribution (solid curves) with the measured data (dotted curves) at two geographical locations: the Equator (blue curves) and the 60°N (red curves).

until the ozone concentration reaches a peak value of 9.41 ppm around  $z = 30$  km. The richest ozone concentration defines the peak of the stratospheric ozone layer.

As the UV ray penetrates through the air mass of the upper stratosphere, its intensity deteriorates due to the absorption by regular oxygen molecules in the photolysis. The weakened UV radiation slows down the generation of atomic oxygen and ozone, while the ozone-depletion reactions of Equations (3), (4), (9), (11), and (12) in **Table 1**, remain effective in destroying the ozone. In the presence of human-induced ozone-depleting chemicals: chlorine, bromine, and  $\text{NO}_x$ , ozone depletion processes continue, especially in the lower stratosphere. Also, other physical processes, such as diffusion and slow air movement, affect the ozone distribution and concentrations. As seen in **Figure 3**, ozone concentration decreases rapidly from the peak at mid-stratosphere to a low boundary value of 0.5 ppm at  $z = 15$  before transitioning to the tropopause and the troposphere below.

For places near 60°N latitude, **Figure 3** shows different calculated (solid red curve) and measured (dotted red curve) ozone concentrations and profiles than those of the Equator. The calculated ozone concentrations reach a smaller peak of 8.25 ppm around  $z = 31.5$  km, while the measured ozone concentrations reach a peak of 7.10 ppm at a higher altitude at  $z = 34.5$  km. The calculated results of our 2-D ozone model generally followed the measured concentrations with the calculated average ozone concentration of 5.24 ppm, being close to the measured average of 5.01 ppm. The ozone distribution profiles basically follow the same trend, but with a coefficient of variation, or the average deviation, of 12.6%.

### 3.2. Monthly Variations of Ozone

In this paper, we delve into the intriguing world of monthly evolution of stratospheric ozone concentrations and distribution at the Equator, a region known for its unique atmospheric conditions. As shown in **Figure 4**, our calculations

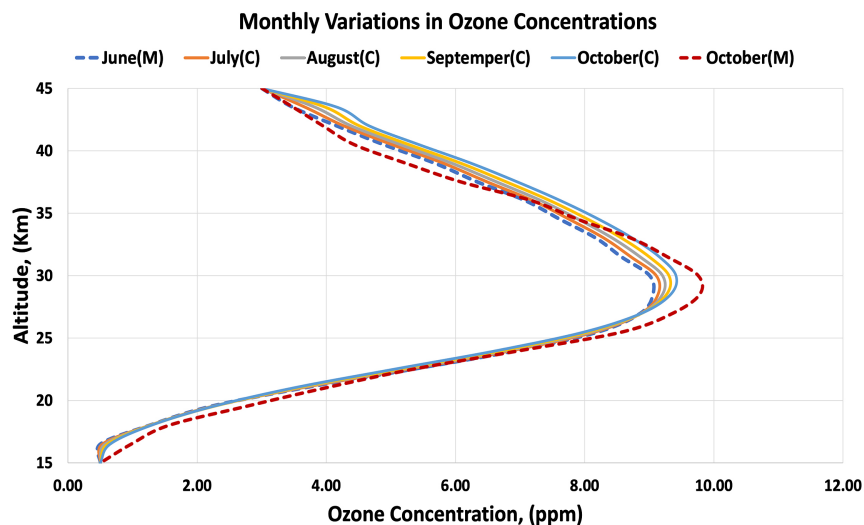


**Figure 4.** Monthly variations of calculated ozone concentrations and distribution from June, July, August, September, to October at the Equator (solid curves), and the comparison with the measured data averaged over 15 years between 2005 and 2019 for months of June and October (dotted curves). The curve labeled with “October (C)” represents the calculated results, while “October (M)” represents the measured data [27].

spanned for five months, from June to October, took into account the typical relatively low values for convection and diffusion, as well as chemical reactions of various atmospheric species commonly encountered in the tropical region [19]. It is noted that in **Figure 4**, our June and October data were also compared to the measured data averaged over 15 years between 2005 and 2019 [27].

As seen in **Figure 4**, the ozone concentrations and distributions for different months aligned closely and followed a similar symmetric profile of 3 ppm at the top stratospheric boundary at  $z = 45$  km, to increase to a peak of the ozone layer in the mid-stratosphere, and to decrease to 0.5 ppm at the bottom stratospheric boundary at  $z = 15$  km. The monthly average ozone concentrations remained within 5% of the mean and were specifically: 5.45 ppm for June (measured), 5.51 ppm for July (calculated), 5.57 ppm for August (calculated), 5.63 ppm for September (calculated), 5.70 ppm for October (calculated), and 5.66 ppm for October (measured). It is noted that a good alignment of the ozone profiles and a small variation within 5% of the average ozone concentrations are understandable for the tropical region of stable environmental conditions and ozone-related reactions. For the polar regions of very low temperatures, specific polar stratospheric clouds, and different non-reactive species serving as random intermediates, the various ozone-depleting reactions in Equations (3), (4), (9), (11), and (12), would play a different dominant role, leading to significant ozone destruction than the Equatorial region.

**Table 2** lists the detailed changes of calculated ozone concentrations along the altitude in the stratosphere at the Equator for five months, from June to October. For data comparison and model validation, **Table 2** also lists the measured data of month of October at the Equator and the  $60^\circ\text{N}$ , close to the North Pole [27].

**Table 2.** Monthly variations of calculated ozone concentrations and distribution from June, July, August, September, to October at the Equator, and the comparison with the measured data averaged over 15 years between 2005 and 2019 for the month of October and for the Equator and the 60°N.

Altitude	Ozone, ppm									
	Equator 0°N					60°N				
	June	July	August	September	October	October	October	October	October	October
Z, km	M	C	C	C	C	M	[(C - M)/M] <sup>2</sup>	C	M	[(C - M)/M] <sup>2</sup>
45	3.00	3.00	3.00	3.00	3.00	3.00	0.000	3.00	3.00	0.000
43.5	3.48	3.67	3.82	3.98	4.16	3.48	0.039	3.56	3.96	0.010
42	4.16	4.27	4.38	4.51	4.66	3.94	0.033	3.91	4.71	0.029
40.5	4.89	5.01	5.14	5.27	5.43	4.43	0.052	4.55	5.39	0.025
39	5.68	5.81	5.94	6.08	6.24	5.23	0.038	5.38	6.18	0.017
37.5	6.34	6.49	6.64	6.79	6.96	6.09	0.021	6.22	6.84	0.008
36	7.09	7.20	7.33	7.46	7.63	7.18	0.004	6.95	7.21	0.001
34.5	7.62	7.77	7.91	8.05	8.22	7.90	0.002	7.60	7.38	0.001
33	8.18	8.30	8.43	8.57	8.74	8.72	0.000	8.07	7.32	0.011
31.5	8.57	8.72	8.86	9.00	9.16	9.28	0.000	8.25	7.10	0.026
30	9.01	9.11	9.21	9.30	9.41	9.76	0.001	8.19	6.73	0.047
28.5	9.06	9.14	9.21	9.27	9.33	9.78	0.002	7.88	6.54	0.042
27	8.87	8.88	8.88	8.89	8.89	9.37	0.003	7.37	6.20	0.035
25.5	8.21	8.16	8.11	8.06	8.01	8.59	0.005	6.71	5.73	0.030
24	6.95	6.87	6.80	6.73	6.65	7.00	0.003	5.85	5.26	0.012
22.5	5.33	5.26	5.19	5.12	5.05	5.33	0.003	4.82	4.75	0.000
21	3.64	3.60	3.56	3.53	3.49	3.97	0.015	3.91	3.80	0.001
19.5	2.19	2.21	2.22	2.23	2.23	2.73	0.034	3.13	2.93	0.005
18	1.26	1.26	1.26	1.27	1.28	1.55	0.030	2.36	2.14	0.011
16.5	0.50	0.53	0.57	0.61	0.65	0.98	0.109	1.79	1.55	0.023
15	0.50	0.50	0.50	0.50	0.50	0.50	0.000	0.50	0.50	0.000
<b>Avg. (ppm)</b>	<b>5.45</b>	<b>5.51</b>	<b>5.57</b>	<b>5.63</b>	<b>5.70</b>	<b>5.66</b>	<b>0.019</b>	<b>5.24</b>	<b>5.01</b>	<b>0.016</b>
<b>Dobson Unit (DU)</b>	<b>320</b>	<b>316</b>	<b>318</b>	<b>321</b>	<b>323</b>	<b>353</b>		<b>297</b>	<b>265</b>	
<b>Coefficient of Variation (%)</b>							<b>13.7%</b>			<b>12.6%</b>

The total abundance of ozone in Dobson Unit (DU) at the Equator can be calculated with values in **Table 2**: 377 DU for June, 374 DU for July, 376 DU for August, 378 DU for September, and 380 DU for October, respectively. The difference of the total ozone abundance between the calculations and the measurements was 7.3% less for the Equator and 11.5% more for the 60°N location.

These DUs provide a good measure of ozone thinning or ozone thickening, including the ozone hole, at different geographical locations and throughout different months of the year.

To calculate the total ozone abundance in DU, a working formula for the weighted integration of altitudinal ozone concentrations  $[O_3]_{ppm}$  is used [1] [7]. This integration considers local variations in air temperature ( $T$ , in degree Kelvin) and total air pressure ( $P$ , in Pascal) within the stratosphere from 15 km to 45 km. The formula is structured as follows:

$$DU = [O_3] \times 6.022 \times 10^{23} \times (P/RT) / (2.69 \times 10^{19}),$$

where  $6.022 \times 10^{23}$  being Avogadro's number or total number of molecules per mole,  $R$  being the universal gas constant. It should be noted here that our calculated ozone abundance is only for the stratosphere (15 km - 45 km), and does not consider ozone in the troposphere, which typically amounts to about 10% of the total abundance.

### 3.3. Influence of Convection: Vertical Speed $U_z$

In this study, our 2-D Ozone Model is used to better understand and quantify the influences of slow air movement, in both  $z$  and  $r$  directions, and the mass diffusivity, of both ozone and atomic oxygen, on ozone concentrations and profile in the stratosphere. Both average dimensionless wind speeds  $U_z$  and  $U_r$  were taken as constant at  $1 \times 10^{-8}$ , or a slow air movement of 20 m/hr, with a reference speed of  $6 \times 10^5$  m/s in the stratosphere. The total computational efforts spanned for one week with a time step of  $\Delta t = 1$  sec, or a total of  $6 \times 10^5$  steps/week.

**Figure 5** shows the influence of slow vertical wind speed  $U_z$  on ozone concentrations and profile of ozone layer in the stratosphere above the Equator. For parametric study of the effects of  $U_z$ , five values of varying dimensionless vertical speed of  $U_z = 0$  (black dotted curve),  $1 \times 10^{-8}$  (blue curve),  $1 \times 10^{-7.5}$  (green curve),  $1 \times 10^{-7}$  (orange curve), and  $1 \times 10^{-6.5}$  (red curve) were selected in the simulations. At zero wind speed  $U_z = 0$ , the ozone distribution followed a symmetric profile as expected, of 3 ppm at the top boundary at  $z^* = 1$  ( $z = 45$  km), a peak of ozone layer of 9.1 ppm at  $z^* = 0.48$  ( $z = 29$  km), and of 0.5 ppm at the bottom boundary at  $z^* = 0$  ( $z = 15$  km).

**Table 3** lists the detailed calculations of ozone concentrations along the altitude in the stratosphere above the Equator, showing the influences of slow vertical wind speed  $U_z$ . As also seen in **Figure 5**, as  $U_z$  increased from zero to  $10^{-6.5}$  (or 0.65 km/hr), the ozone concentrations and the profile remained about the same, but with an upward shift of the peak, from  $z^* = 0.48$  at 29 km to  $z^* = 0.6$  at  $z = 33$  km, in the stratosphere. This upward shift of similar ozone distribution profile at higher  $U_z$  seemed to keep the area enclosed between the curve and  $z^*$  axis the same. However, the total ozone abundance calculated from the weighted integration of the area would decrease, from 320 DU at  $U_z = 0$ , to 313 DU at  $U_z$

=  $10^{-8}$ , to 296 DU at  $U_z = 10^{-7.5}$ , to 249 DU at  $U_z = 10^{-7}$ , and to 211 DU at  $U_z = 10^{-6.5}$ . The slow upward air motion in the thermally stable stratosphere simply blew the ozone-lean air mass from the lower stratosphere to the higher altitude in one week time above the Equator.

**Table 3.** Calculated ozone concentrations in the stratosphere above the Equator, showing the influences of slow vertical wind speed  $U_z$ .

Influence of Vertical/Upward Velocity, $U_z$					
Normalized Altitude, $z$	Ozone Concentration (ppm)				
	$U_z = 0$	$U_z = 10^{-8}$	$U_z = 10^{-7.5}$	$U_z = 10^{-7}$	$U_z = 10^{-6.5}$
1.00	3.00	3.00	3.00	3.70	4.87
0.95	3.48	3.54	3.71	4.37	5.63
0.90	4.15	4.23	4.42	5.03	6.39
0.85	4.88	4.97	5.17	5.79	7.03
0.80	5.67	5.76	5.95	6.51	7.64
0.75	6.34	6.42	6.60	7.14	8.16
0.70	7.08	7.16	7.32	7.79	8.59
0.65	7.62	7.68	7.81	8.20	8.85
0.60	8.17	8.22	8.34	8.69	9.06
0.55	8.56	8.61	8.71	8.94	8.77
0.50	9.00	9.03	9.07	9.08	8.21
0.45	9.05	9.04	9.00	8.71	7.01
0.40	8.87	8.81	8.67	8.01	5.56
0.35	8.22	8.10	7.82	6.75	3.79
0.30	6.95	6.78	6.38	5.05	2.23
0.25	5.34	5.14	4.71	3.40	1.21
0.20	3.64	3.46	3.07	1.98	0.52
0.15	2.19	2.05	1.76	1.04	0.34
0.10	1.26	1.16	0.98	0.55	0.29
0.05	0.50	0.46	0.38	0.27	0.37
0.00	0.50	0.50	0.50	0.50	0.50
<b>Average</b>	<b>5.45</b>	<b>5.43</b>	<b>5.40</b>	<b>5.31</b>	<b>5.00</b>
<b>Total Ozone Abundance, DU</b>	<b>320</b>	<b>313</b>	<b>296</b>	<b>249</b>	<b>211</b>
<b>Coeff. of Variations, %</b>		<b>0.29%</b>	<b>0.95%</b>	<b>2.59%</b>	<b>8.25%</b>

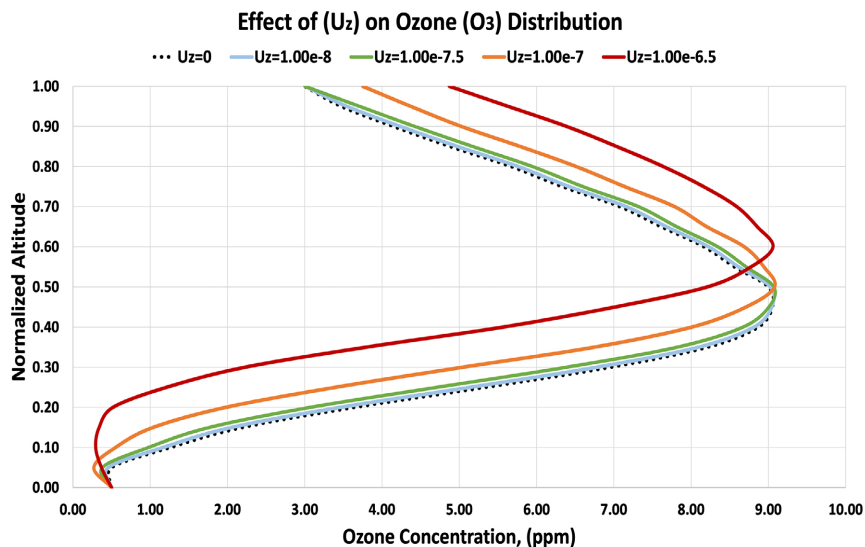


**Figure 5.** Influence of slow vertical wind speed  $U_z$  on stratospheric ozone concentrations and profile of ozone layer above the Equator.

### 3.4. Influence of Convection: Horizontal Radial Speed $U_r$

This section delves into the impact of horizontal radial air movement  $U_r$  on stratospheric ozone concentrations and profile. **Figure 6** shows the influence of slow horizontal radial wind speed  $U_r$  on ozone concentrations and profile of ozone layer in the stratosphere above the Equator. Five values of dimensionless radial speed of  $U_r = 1 \times 10^{-9}$  (black dotted curve),  $1 \times 10^{-8.5}$  (blue curve),  $1 \times 10^{-8}$  (green curve),  $1 \times 10^{-7.5}$  (orange curve), and  $1 \times 10^{-7}$  (red curve) were selected in the simulations. All ozone concentration distributions exhibited similar symmetric profiles of 3 ppm at the top boundary at  $z^* = 1$  ( $z = 45$  km), a peak of ozone layer of different values at the mid-stratosphere  $z^* = 0.45$  ( $z = 28$  km), and of 0.5 ppm at the bottom boundary at  $z^* = 0$  ( $z = 15$  km).

As shown in **Figure 6**, as  $U_r$  increased from zero to  $10^{-7}$  (or 0.2 km/hr), the ozone concentrations profiles remained the same, but the peak concentrations at  $z^* = 0.45$  ( $z = 29$  km) of 9.05 ppm for  $U_r = 0$  decreased gradually to 7.62 ppm for  $U_r = 1 \times 10^{-7}$ . The average concentrations in the stratosphere decreased from 5.45 ppm (100%) for  $U_r = 0$  to 4.70 ppm (86%) for  $U_r = 1 \times 10^{-7}$ .

The slow radial air motion in the stratosphere did not change the altitudinal ozone concentrations and profile much; however its impacts on radial ozone concentrations and distribution were evident and thereby discussed below.

**Figure 7** plots the calculated ozone concentrations and distribution profiles along the normalized radial coordinate,  $r^* = 0$  to 1, above the Equator for different altitudes:  $z = 15$  km (bottom diagram),  $z = 30$  km (middle diagram), and  $z = 45$  km (top diagram), and for different elapsed times of the wind blow: 1 day (blue curve), 3 days (orange curve), and 1 week (green curve). In the bottom diagram in **Figure 7** ( $z = 15$  km), the ozone concentration after 1 day (blue curve) of slow wind blow of  $U_r = 1 \times 10^{-7}$ , increased from the boundary value of 0.5 ppm at  $r^* = 0$  to 1 ppm. It increased gradually to 2.3 ppm at  $r^* = 0.25$ , and then

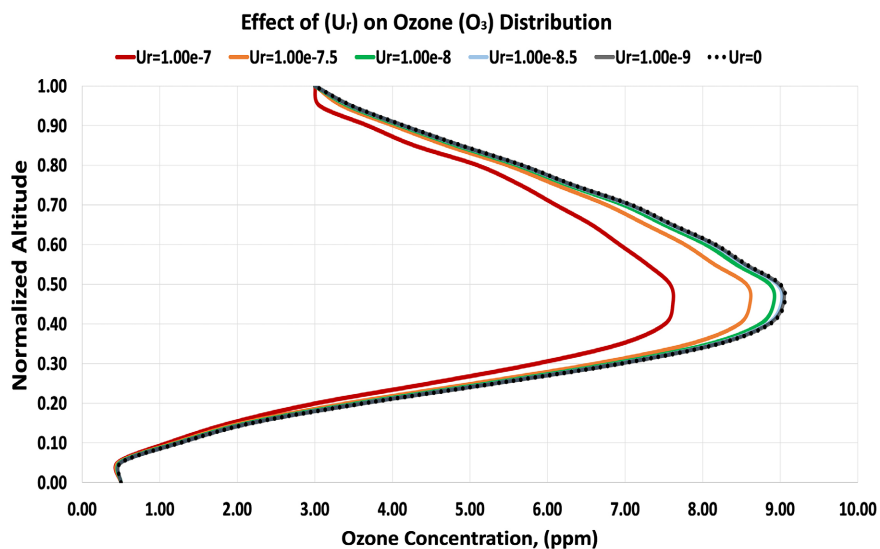


**Figure 6.** Influence of slow horizontal radial wind speed  $U_r$  on stratospheric ozone concentrations and profile of ozone layer above the Equator.

dropped to 1.2 ppm at  $r^* = 0.47$ , and then increased again to 2.5 ppm at  $r^* = 0.9$  and onwards. The fluctuation in ozone concentration showed that it didn't maintain a monotonous pattern across all radial locations at this altitude. Additionally, the change in ozone concentrations evolved over time periods of 1 day, 3 days, and 1 week exhibited the similar profiles, but shifted towards the right. As expected, the right-shifting ozone profiles correlated well with the radial wind movement  $U_r$  blowing to larger  $r^*$ .

The middle diagram of **Figure 7** showed the radial ozone concentrations in the mid-stratosphere at  $z = 30$  km. As expected, the ozone concentrations were comparatively higher, up to 9 ppm around  $r^* = 0.58$  for  $t = 1$  day (blue curve). The distribution profiles for different elapsed time of 1 day, 3 days, or 1 week exhibited a smoother curve that closely resembled straight lines. Results also showed that as the radial wind speeds decreased with  $U_r < 10^{-7}$ , the radial ozone profiles becoming closer with less separation between the three curves, which reduced the sensitivity of ozone concentrations to the influence of  $U_r$  and the impact of convection. The top diagram of **Figure 7** showed the radial ozone concentrations near in the upper stratosphere at  $z = 45$  km. The peak concentrations of 5 ppm around  $r^* = 0.28$  for  $t = 1$  day (blue curve), 4 ppm at  $r^* = 0.32$  for  $t = 3$  days (orange curve), and 3 ppm at  $r^* = 0.41$  for  $t = 1$  week (green curve).

### 3.5. Influence of Gas Diffusion: Diffusivity of Ozone $D_{O_3}$

In this section, we aim at exploring the diffusion of ozone gases ( $O_3$ ) and atomic oxygen gases (O) on ozone concentrations and distribution in the stratosphere. It's noted that the measured concentration data for ozone and atomic oxygen above the equatorial region were taken from the publicly known source of Dr. William [20]. To investigate the influence of gas diffusivities on ozone concentrations, and to compare them to the known data, we converted the unit of

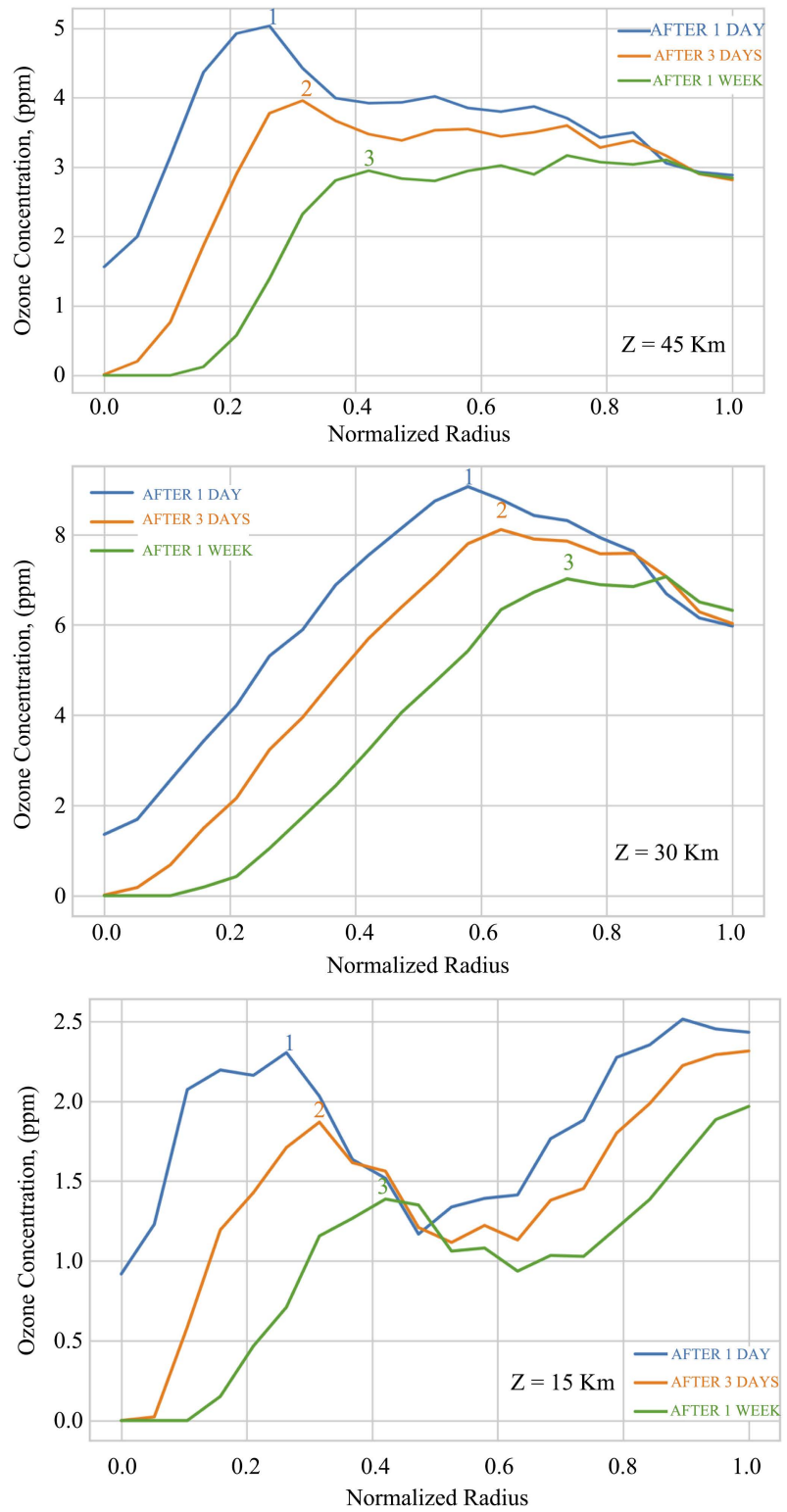


**Figure 7.** Calculated ozone concentrations and distribution profiles along the radial direction above the Equator for different altitudes:  $z = 15 \text{ km}$  (lower diagram),  $z = 30 \text{ km}$  (middle diagram), and  $z = 45 \text{ km}$  (upper diagram), and for different elapsed times for radial wind movement of  $U_r = 1 \times 10^{-7}$ : 1 day (blue curve), 3 days (orange curve), and 1 week (green curve).

ozone concentrations from ppm to molecules/cm<sup>3</sup> (mol/cm<sup>3</sup>). The change in concentration units may induce alterations in the observed ozone peak, potentially shifting it downwards.

**Figure 8** shows the influence of diffusivity of ozone gas  $D_{O_3}$  on ozone concentrations and profile of the ozone layer at the Equator. A parametric study with five different values of  $D_{O_3}$ , ranging from publicly known value of  $1 \times 10^{-9.5}$  to a 3160 fold value of  $1 \times 10^{-6}$ : black curve for  $D_{O_3} = 10^{-9.5}$ , blue curve for  $D_{O_3} = 10^{-9}$ , green curve for  $D_{O_3} = 10^{-8}$ , yellow curve for  $D_{O_3} = 10^{-7}$ , and red curve for  $D_{O_3} = 10^{-6}$ . With gas diffusivity of ozone  $D_{O_3} = 10^{-9.5}$  (black curve), the ozone concentration at the top boundary ( $z^* = 1, z = 45$  km), was taken as 3 ppm, or equivalently  $1.35 \times 10^{11}$  mol/cm<sup>3</sup>. A peak value of the ozone distribution of  $3.38 \times 10^{12}$  mol/cm<sup>3</sup> (or 5.34 ppm) was found in the lower stratosphere at  $z^* = 0.25$  ( $z = 23$  km), which was different from the peak value in 9.05 ppm at  $z^* = 0.45$  ( $z = 29$  km). The shifting of the representing peak of the ozone layer is expected because molecules per volume (mol/cm<sup>3</sup>) is an absolute concentration unit, while parts per million (ppm) is a relative concentration unit changing with the local air density, pressure and temperature. At the bottom boundary  $z^* = 0, (z = 15$  km), was taken as 0.5 ppm, or equivalently  $1.6 \times 10^{12}$  mol/cm<sup>3</sup>.

**Figure 8** shows the influence of diffusivity of ozone gas  $D_{O_3}$  on ozone concentrations and profile of the ozone layer. As seen in **Figure 8**, the ozone profiles changed to lesser non-uniform shape of distribution from smaller diffusivity  $D_{O_3}$  (black curve,  $10^{-9.5}$ ), to small  $D_{O_3}$  (blue curve,  $10^{-9}$ ), to intermediate  $D_{O_3}$  (green curve,  $10^{-8}$ ), to large  $D_{O_3}$  (yellow curve,  $10^{-7}$ ), and to very large  $D_{O_3}$  of uniform straight line (red curve,  $10^{-6}$ ). The location and peak value of ozone distributions shifted slightly from  $3.38 \times 10^{12}$  mol/cm<sup>3</sup> at  $z^* = 0.25$  to the lower stratosphere of  $2.0 \times 10^{12}$  mol/cm<sup>3</sup> close to  $z^* = 0$ . A large diffusivity with strong gas diffusion made the profile more uniform as expected. While the average ozone concentrations remained almost a constant around to 5.4 ppm, the total ozone abundance increased slightly, but around 340 DU. It is also noted that the results in **Figure 8** are for ozone concentrations with both physical processes (diffusion and

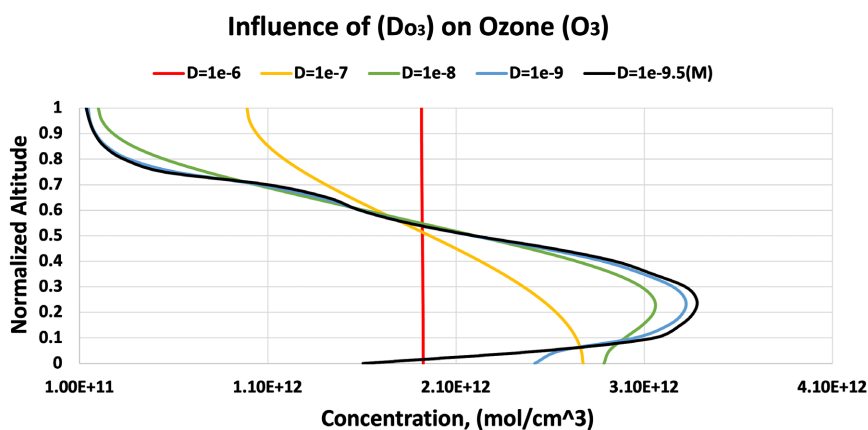


**Figure 8.** Influence of diffusivity of ozone gas  $D_{O_3}$  on ozone concentrations and profile of the ozone layer above the Equator.

convection) and chemical processes (natural ozone processes, Equations (1) to (3), and human-induced ozone-depletion processes Equations (4) to (14)) considered. Another series of numerical simulations without man-made ozone depletions (or Equations (4) to (14) setting to zero) showed that the influence of ozone diffusivity  $D_{O_3}$  on ozone concentrations and profile is not much different from that with chemical reactions seen in **Figure 8**.

### 3.6. Influence of Gas Diffusion: Diffusivity of Atomic Oxygen $D_O$

Now, turning our attention to **Figure 9**, we delve deeper into the influence of physical diffusion of  $D_O$  and atomic oxygen-related chemical reactions on the concentrations and distribution of ozone and also atomic oxygen in the stratosphere. We started with an original, measured ozone profile with a base diffusivity of atomic oxygen of  $D_O = 10^{-8}$ , (black curve) [20]. The calculations of mass balance equations of ozone  $O_3$  as well as atomic oxygen  $O$  with all 14 chemical reaction equations considered (see **Table 1**) for an elapsed time of one week.

As seen in **Figure 9**, as time elapsed, the ozone profiles changed to a more uniform shape of distribution from smaller diffusivity of 50%  $D_O$  ( $=0.5 \times 10^{-8}$ , blue curve), to intermediate value of 100%  $D_O$  ( $1 \times 10^{-8}$ , green curve), to large value of 200%  $D_O$  ( $2 \times 10^{-8}$ , yellow curve), and to very large value of 400%  $D_O$  ( $4 \times 10^{-8}$ , red curve). A larger diffusivity with stronger atomic oxygen gas diffusion made the profile more uniform as expected. However, different from the influence of ozone diffusivity  $D_{O_3}$  in **Figure 8**, as  $D_O$  increased, the ozone distribution shifted from having a distinct peak at  $z^* = 0.25$  quickly to a more flattened curve with peaks close to the bottom boundary of the stratosphere at  $z^* = 0$ . The ozone distribution at the atomic oxygen diffusivity  $D_O = 0.5 \times 10^{-8}$  (blue curve) exhibited a 7% increased concentration at the peak of  $3.38 \times 10^{12}$  mol/cm<sup>3</sup>, and the shifted peak got close to the bottom of the stratosphere.

To better understand the physical and chemical processes causing the above interesting observation, **Figure 10** plots the effect of atomic oxygen diffusivity  $D_O$  on the concentrations and distribution of atomic oxygen above the equatorial

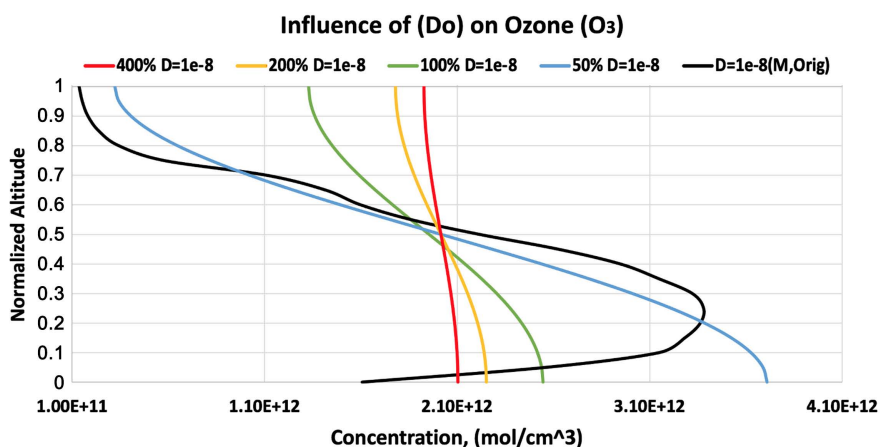


**Figure 9.** Influence of diffusivity of atomic oxygen gas  $D_O$  on ozone concentrations and profile of the ozone layer above the equatorial region.

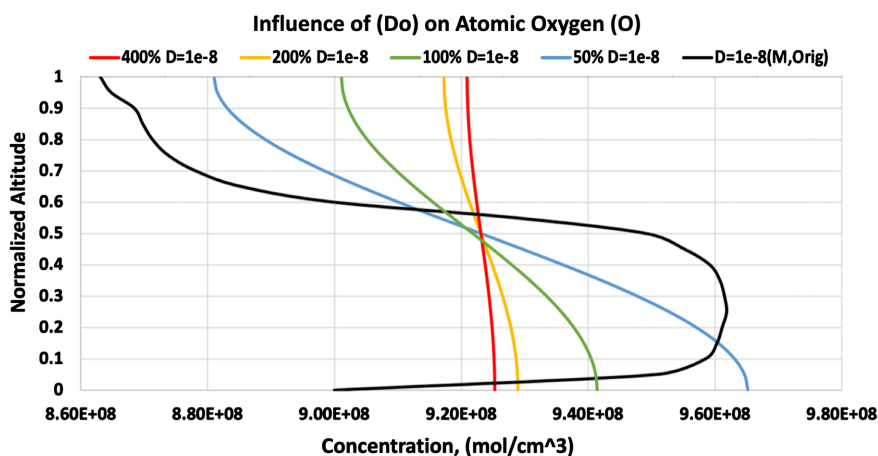


**Figure 10.** Effect of diffusivity of atomic oxygen gas  $D_{O}$  on concentrations and distribution of chemically active atomic oxygen above the equatorial region.

region. The measured atomic oxygen profile with a base diffusivity of atomic oxygen of  $D_{O} = 10^{-8}$ , (black curve) was used for transient calculations for an elapsed time of one week [20]. **Figure 10** showed the effect of  $D_{O}$  on its concentrations and profile, considering the mass balance equation of atomic oxygen along with all 14 ozone-depletion related chemical equations (see **Table 1**).

As time elapsed, the atomic oxygen profiles, again under five different values of  $D_{O}$ , changed to a more uniform shape of distribution from smaller diffusivity of 50%  $D_{O}$  ( $=0.5 \times 10^{-8}$ , blue curve), to intermediate value of 100%  $D_{O}$  ( $1 \times 10^{-8}$ , green curve), to large value of 200%  $D_{O}$  ( $2 \times 10^{-8}$ , yellow curve), and to very large value of 400%  $D_{O}$  ( $4 \times 10^{-8}$ , red curve). A larger diffusivity with stronger atomic oxygen diffusion made the atomic oxygen profiles more uniform as expected. It is clearly seen that as  $D_{O}$  increased, the bell-shaped atomic oxygen distribution (black curve) shifted quickly from having a distinct peak of  $9.62 \times 10^8$  mol/cm<sup>3</sup> at  $z^* = 0.25$  to a more uniform S-shaped profile (blue curve) with the peak found at the bottom boundary of the stratosphere ( $z^* = 0$ ). The peak concentration of atomic oxygen for  $D_{O} = 0.5 \times 10^{-8}$  (blue curve) exhibited a 1% increase in concentration of  $9.67 \times 10^8$  mol/cm<sup>3</sup>. As  $D_{O}$  further increased, the S-shaped profiles in **Figure 10**, evolved from blue to green, to yellow, and to red curves of more uniform and flattened distributions, converging to  $9.23 \times 10^8$  mol/cm<sup>3</sup>, as expected.

It is known that different properties of  $D_{O}$  (also  $D_{O_3}$ ) diffusivity would dictate different levels of strong or weak physical diffusion in space of atomic oxygen (or ozone) concentrations in the stratosphere (see **Figure 10**). However, the spatial distribution of atomic oxygen in stratosphere would further dictate the amount of ozone increase through natural ozone-generating process as in Equation (2) in **Table 1**, and also different levels of strong or weak ozone-depleting chemical reactions, such as Equations (5) and (4) of chlorine-caused ozone decrease, and Equations (10) and (9) of  $NO_x$ -caused ozone decrease (see **Table 1**). Therefore, the diffusivity of ozone  $D_{O_3}$  only affects the distribution of ozone in

stratosphere by simple physical diffusion. But the diffusivity of atomic oxygen  $D_O$  impacts on the distribution of ozone in stratosphere by both physical diffusion as well as many ozone-producing and ozone-depleting chemical reactions involving atomic oxygen. In summary, the diffusivity (and diffusion) of atomic oxygen was found to be more sensitive and important than the diffusivity (and diffusion) of ozone on stratospheric ozone concentrations and distribution (ozone layer).

#### 4. Summary

An engineering system approach of 2-D cylindrical model of transient mass balance calculations of ozone and other concerned chemicals along with fourteen photolysis, ozone-generating and ozone-depleting chemical reaction equations was developed, validated, and used for studying the ozone concentrations, distribution and peak of the layer, ozone depletion and total ozone abundance in the stratosphere. The calculated ozone concentrations and profile along the altitude at both the Equator and high-latitude location at  $60^\circ\text{N}$  were found to exhibit a more symmetrical distribution along the altitude with a peak concentration of 9.41 ppm near the mid-altitude at  $z = 30$  km, as compared to the measured ozone concentrations of a similar symmetrical distribution with a peak concentration of 9.76 ppm near  $z = 30$  km. The calculated results of our 2-D ozone model generally followed the measured concentrations with the calculated average ozone concentration of 5.77 ppm, being very close to the measured average of 5.66 ppm. The ozone distribution profiles follow the same trend but with a coefficient of variation, or the average deviation, of 13.7%.

The monthly evolution of stratospheric ozone concentrations and distribution above the Equator were studied, spanning for five months, from June to October. The calculated results were compared to and validated by the measured data, averaged over 15 years between 2005 and 2019. The calculated ozone concentrations for different months aligned closely and followed a similar symmetric profile of 3 ppm at the top stratospheric boundary at  $z = 45$  km, to increase to a peak of the ozone layer in the mid-stratosphere, and to decrease to 0.5 ppm at the bottom stratospheric boundary at  $z = 15$  km. The calculated monthly average ozone concentrations were found to be in good agreement with the measured ozone concentrations within 5% of deviation for the tropical region. The total abundance of ozone in Dobson Unit (DU) at the Equator were calculated to be 377 DU for June, 374 DU for July, 376 DU for August, 378 DU for September, and 380 DU for October, respectively. The difference of the total ozone abundance between the calculations and the measurements was  $-7.3\%$  for the Equator and  $11.5\%$  for the  $60^\circ\text{N}$  location. These calculated DUs provide a good measure of ozone thickening or thinning, including the ozone hole, at different geographical locations and throughout different months of the year.

The influences of slow air movement in both  $z$  and  $r$  directions on ozone concentrations and profile in the stratosphere were investigated. As the vertical

wind speed  $U_z$  increased, the ozone concentrations and the profile remained almost the same, but with an upward shift of the peak, from mid-altitude of  $z = 29$  km to  $z = 33$  km in the upper stratosphere. The slow upward air motion in the thermally stable stratosphere were found to simply blow the ozone-lean air mass from the lower stratosphere to the higher altitude as expected. The influence of slow horizontal radial wind speed  $U_r$  on ozone concentrations and profile of ozone layer was also studied with five different radial speeds of  $U_r$ . As  $U_r$  increased, the ozone concentrations profiles remained about the same, but the peak concentrations around the mid-altitude at  $z = 29$  km of 9.05 ppm for  $U_r = 0$  decreased gradually to 7.62 ppm for large  $U_r = 1 \times 10^{-7}$ , with the average concentrations in the stratosphere decreased about 14%. The slow radial air motion in the stratosphere wouldn't change the altitudinal ozone concentrations and profile much; however it would impact on radial ozone concentrations and distribution.

The influence of mass diffusivities of both ozone gas  $D_{O_3}$  and active atomic oxygen gas  $D_O$  on ozone concentrations (in molecules/cm<sup>3</sup> instead of ppm) and distribution profile above the Equator were investigated. Parametric studies with five different values of  $D_{O_3}$  covering three orders of magnitude from  $10^{-9.5}$  to  $10^{-6}$ , and five different values of  $D_O$  covering one order of magnitude from 50% to 400% were conducted. The ozone profiles evolved gradually to more uniform shape of distributions as  $D_{O_3}$  or the physical diffusion increased, as expected. The location and peak value of ozone distributions were found to shift slightly from  $3.38 \times 10^{12}$  mol/cm<sup>3</sup> at  $z^* = 0.25$  to the lower stratosphere of  $2.0 \times 10^{12}$  mol/cm<sup>3</sup> close to  $z^* = 0$ .

Different from the influence of  $D_{O_3}$ , as  $D_O$  increased, the ozone distribution shifted from having a distinct peak at  $z^* = 0.25$  quickly to a more flattened curve with peaks close to the bottom boundary of the stratosphere at  $z^* = 0$ . The ozone distribution for  $D_O = 0.5 \times 10^{-8}$  exhibited a 7% increase in ozone concentration of the peak of  $3.38 \times 10^{12}$  mol/cm<sup>3</sup>, and the peak shifted quickly to the bottom of the stratosphere. **Figure 10** further investigated the effect of atomic oxygen diffusivity  $D_O$  on the concentrations and profile of atomic oxygen. It is clearly seen that as  $D_O$  increased, the bell-shaped atomic oxygen distribution shifted quickly from having a distinct peak at  $z^* = 0.25$  to a more uniform S-shaped profiles with the peaks at the bottom boundary of the stratosphere ( $z^* = 0$ ). As  $D_O$  further increased, the S-shaped profiles changed to more uniform and flattened distributions, as expected. Having influences through both physical diffusion and chemical reactions, the diffusivity (and diffusion) of atomic oxygen  $D_O$  was found to be more sensitive and important than the diffusivity (and diffusion) of ozone  $D_{O_3}$  on stratospheric ozone concentrations and distribution (ozone layer).

In summary, this paper presents a robust 2-D Model for analyzing the dynamics of stratospheric ozone, considering the pertinent competing processes of convective transport, mass diffusion, photolysis, ozone-generating and ozone-depleting reactions. The calculated results were validated in generally good

agreement with the published measurement data. This model is convenient, efficient, and executable to study the complex ozone phenomena in the stratosphere.

## Acknowledgements

The authors would like to thank the insightful discussions with colleagues of the Catholic University of America's Climate Change Initiatives of Engineering Center for Care of Earth.

## Conflicts of Interest

The authors declare no conflicts of interest regarding the publication of this paper.

## References

- [1] Salawitch, R.J., McBride, L.A., Thompson, C.R., Fleming, E.L., McKenzie, R.L., Rosenlof, K.H., Doherty, S.J. and Fahey, D.W. (2023) Twenty Questions and Answers about the Ozone Layer: 2022 Update, Scientific Assessment of Ozone Depletion: 2022. World Meteorological Organization, UNEP, NOAA, NASA, and EC, Geneva, 75 pp.
- [2] Wei, L., Alelmi, I. and Nieh, S. (2023) Calculations of Stratospheric Ozone and Effects of Diffusivity. *Atmospheric and Climate Sciences*, **13**, 385-400. <https://doi.org/10.4236/acs.2023.133021>
- [3] U.S. Environmental Protection Agency (2019) Ozone Layer Protection. <https://www.epa.gov/ozone-layer-protection>
- [4] Anwar, F., Chaudhry, F., Nazeer, S., Zaman, N. and Azam, S. (2016) Causes of Ozone Layer Depletion and Its Effects on Human. *Atmospheric and Climate Sciences*, **6**, 129-134. <https://doi.org/10.4236/acs.2016.61011>
- [5] Earth System Research Laboratory (2019) The NOAA Ozone Depleting Gas Index: Guiding Recovery of the Ozone Layer. <https://www.esrl.noaa.gov/gmd/odgi/>
- [6] Wei, L., Alelmi, I. and Nieh, S. (2024) Effects of Chlorine and Chlorine Monoxides on Stratospheric Ozone Depletion. *Atmospheric and Climate Sciences*, **14**, 136-153. <https://doi.org/10.4236/acs.2024.141009>
- [7] Alelmi, I., Wei, L. and Nieh, S. (2023) Modelling, Validation, and Calculations of Stratospheric Ozone Dynamics and Latitudinal Changes. *Journal of Environmental Science and Engineering*, **B12**, 265-279. <https://doi.org/10.17265/2162-5263/2023.06.003>
- [8] Molina, M.J. and Rowland, F.S. (1974) Stratospheric Sink for Chlorofluoromethanes: Chlorine Atom-Catalysed Destruction of Ozone. *Nature*, **249**, 810-812. <https://doi.org/10.1038/249810a0>
- [9] Newman, P.A. and Lait, L.R. (2023) NASA Ozone Watch-Images, Data, and Information for Atmospheric Ozone. NASA-Goddard Space Flight Center, Greenbelt. [https://ozonewatch.gsfc.nasa.gov/scripts/big\\_image.php?date=2023-05-18&hem=s&section=home](https://ozonewatch.gsfc.nasa.gov/scripts/big_image.php?date=2023-05-18&hem=s&section=home)
- [10] Chapman, S. (1930) A Theory of Upper Atmospheric Ozone. *Memoirs of the Royal Meteorological Society*, **3**, 103-125.
- [11] Steed, J.M., Owens, A.J., Miller, C., Filkin, D.L. and Jesson, J.P. (1982) Two-Dimensional Modelling of Potential Ozone Perturbation by Chlorofluorocarbons.

- Nature*, **295**, 308-311. <https://doi.org/10.1038/295308a0>
- [12] Vupputuri, R.K.R. (1989) 2-D Model Simulations of Anomalous Spring Variations of Ozone, Temperature and Other Minor Trace Constituents in the Southern Polar Region. *Atmosphere-Ocean*, **27**, 728-738. <https://doi.org/10.1080/07055900.1989.9649364>
- [13] Grooß, J., Brühl, C. and Peter, T. (1998) Impact of Aircraft Emissions on Tropospheric and Stratospheric Ozone. Part I: Chemistry and 2-D Model Results. *Atmospheric Environment*, **32**, 3173-3184. [https://doi.org/10.1016/S1352-2310\(98\)00016-8](https://doi.org/10.1016/S1352-2310(98)00016-8)
- [14] Holton, J.R. and Wehrbein, W.M. (1980) A Numerical Model of the Zonal Mean Circulation of the Middle Atmosphere. *Pure and Applied Geophysics*, **118**, 284-306. <https://doi.org/10.1007/BF01586455>
- [15] Waugh, D.W., Oman, L., Newman, P.A., *et al.* (2009) Effect of Zonal Asymmetries in Stratospheric Ozone on Simulated Southern Hemisphere Climate Trends. *Geophysics Research Letter*, **36**, L18701. <https://doi.org/10.1029/2009GL040419>
- [16] Coopmann, O., Fourrié, N. and Guidard, V. (2022) Analysis of MTG-IRS Observations and General Channel Selection for Numerical Weather Prediction Models. *Quarterly Journal of the Royal Meteorological Society*, **148**, 1864-1885. <https://doi.org/10.1002/qj.4282>
- [17] Balashov, N.V., Thompson, A.M. and Young, G.S. (2017) Probabilistic Forecasting of Surface Ozone with a Novel Statistical Approach. *Journal of Applied Meteorology and Climatology*, **56**, 297-316. <https://doi.org/10.1175/JAMC-D-16-0110.1>
- [18] Fogler, H.S. (2006) Elements of Chemical Reaction Engineering (Prentice-Hall International Series in the Physical and Chemical Engineering Sciences). 4th Edition, Pearson, Upper Saddle River, New Jersey.
- [19] Chakrabarti, A.K., De Obeso, A., Gürmen, N.M. and Fogler, H.S. (2021) The Kinetics of Ozone Depletion. University of Michigan, Ann Arbor. [http://websites.umich.edu/~elements/6e/web\\_mod/ozone/index.htm](http://websites.umich.edu/~elements/6e/web_mod/ozone/index.htm)
- [20] William, H. (1995) Chapter 7: Stratospheric Chemistry, Meteorology 532-Stratospheric Chemistry. [https://personal.ems.psu.edu/~brune/m532/meteo532\\_ch7\\_stratospheric\\_chemistry.htm](https://personal.ems.psu.edu/~brune/m532/meteo532_ch7_stratospheric_chemistry.htm)
- [21] Cooper, C.D. and Alley, F.C. (2011) Chapter 16: Control of Nitrogen Oxides. In: Cooper, C.D. and Alley, F.C., Eds., *Air Pollution Control: A Design Approach*, 4th Edition, Waveland Press, Prospect Heights, 523-555.
- [22] Chen, J.R. and Nieh, S. (1995) SO<sub>2</sub> and NO<sub>x</sub> Control in a Pulverized Coal-Fired Vortex Combustor. *Proceedings of the 20th International Technical Conference on Coal Utilization and Fuel Systems*, Clearwater, 20-23 March 1995, 311-322.
- [23] Salman, A.K., Pouyaei, A., Choi, Y., Lops, Y. and Sayeed, A. (2022) Deep Learning Solver for Solving Advection-Diffusion Equation in Comparison to Finite Difference Methods. *Communications in Nonlinear Science and Numerical Simulation*, **115**, Article 106780. <https://doi.org/10.1016/j.cnsns.2022.106780>
- [24] Brasseur, G. and Solomon, S. (1986) *Aeronomy of the Middle Atmosphere*. D. Reidel Publishing Company, Dordrecht.
- [25] Mori, C. and Romão, E.C. (2021) Numerical Simulation by Finite Difference Method of 2D Convection-Diffusion in Cylindrical Coordinates. [https://www.researchgate.net/publication/306318916\\_numerical\\_simulation\\_by\\_finite\\_difference\\_method\\_of\\_2d\\_convection-diffusion\\_in\\_cylindrical\\_coordinates](https://www.researchgate.net/publication/306318916_numerical_simulation_by_finite_difference_method_of_2d_convection-diffusion_in_cylindrical_coordinates)

- [26] Buckman, N.M. (2016) The Linear Convection-Diffusion Equation in Two Dimensions. Massachusetts Institute of Technology Course 18.303 Linear Partial Differential Equations, Cambridge.
- [27] Tang, Q., Prather, M.J., Hsu, J., Ruiz, D.J., Cameron-Smith, P.J., Xie, S. and Golaz, J.C. (2016) Evaluation of the Interactive Stratospheric Ozone (O3v2) Module in the E3SM Version 1 Earth System Model. *Geoscientific Model Development*, **14**, 1219-1236. <https://doi.org/10.5194/gmd-14-1219-2021>